

Tomography Using a Rotating Slant-Hole Collimator and a Large Number of Projections

Susanne Dale and Dianna Bone

Department of Medical Engineering, Karolinska Institute, Huddinge, Sweden and Department of Clinical Physiology, Thoracic Clinics, Karolinska Hospital, Stockholm, Sweden

A tomographic method using a limited-view angle has been evaluated. In studies using a gamma camera and a rotating 30-degree slant-hole (RSH) collimator, 64 projection images were registered. A special filtered backprojection technique was used for reconstruction of section images parallel to the collimator face. Resolution within such sections was 0.6 cm, 3 cm from the collimator face and 1.3 cm at 18 cm. Depth resolution was 2.2 cm at 3 cm and 5.1 cm at 18 cm. Spacing between section images was regular and geometric distortion negligible. Short-axis section images of a myocardium in vivo were qualitatively comparable or better than those obtained with single-photon emission computed tomography. Degradation in the posterior wall due to attenuation and scatter was less. Section images of the facial bones and a hip joint further demonstrated the tomographic capability of the method.

J Nucl Med 1990;31:1675-1681

A tomographic method in which projection data are acquired from a restricted-view angle is presented. The method was originally developed for use in radiographic imaging (1-3) but is currently being implemented in gamma camera imaging (4). The camera can be angled and rotated according to the desired direction of projection or a rotating slant-hole (RSH) collimator can be used.

Tomography using a RSH collimator was first presented in gamma camera imaging in 1970 (5,6). Since then, some thirty papers have appeared describing rotating slant-hole tomography (RSHT) (7-23).

The acquisition procedure of RSHT results in several two-dimensional images, i.e., projections, of an object. Images are obtained by a parallel projection of the object to different locations spaced at equal intervals around the circle described by the rotation of the slant-hole collimator; the projection circle. The view angle,

i.e., the slant of the collimator, is usually between 21.5° and 45°, the smaller angle resulting in a larger reconstruction volume; the larger angle in a better depth resolution. The reconstruction volume is the volume of the object intersected by all projections; the volume outside it is only partially viewed and details here will be imaged with less resolution and contrast.

The tomographic method presented differs from earlier slant-hole methods in the number of projection images acquired and the reconstruction algorithm employed. Instead of using only six or eight projections and an iterative reconstruction algorithm (8-12,14-17,19-23), at least 60 projections and a filtered backprojection technique are used. A large number of projections yields a more complete angular sampling and, furthermore, is necessary in two-dimensional filtered backprojection to efficiently eliminate out-of-section activity.

All systems for RSHT and conventional tomography are restricted to a view angle less than 90°. When the three-dimensional Fourier transforms are calculated for both the projected object and its projection images, the transforms will not be identical (2). There is a volume, shaped as an inverted double cone with an axis coinciding with the axis of rotation, in which data are missing. This volume is therefore often called the empty cone. The empty cone limits restricted-view angle methods (24-26): reconstruction of a strictly quantitative section image is impossible and resolution between section images is relatively poor. In theory, quantitative section images can be reconstructed using single-photon emission computed tomography (SPECT), but in some applications, resolution and signal-to-noise ratio (SNR) are comparatively poor because of scatter and attenuation. In these applications, RSHT can be qualitatively superior because of an advantageous acquisition geometry. Such a geometry is obtained when the organ of interest is situated close and parallel to the body surface. RSHT has until now been used for imaging the myocardium (18-12,16,18,20-23), femoral neck fractures (13), cerebral blood flow (14,15,17), and the spleen (19), but other organs such as the thyroid, the bones of the hand, the knee joint, and the spine are also advanced.

Received Feb. 9, 1989; revision accepted Mar. 26, 1990.

For reprints contact: Susanne Dale, PhD, Department of Medical Engineering, F60, Karolinska Institute Novum, Huddinge University Hospital, S-14186 Huddinge, Sweden.

tageous, especially if more than eight projections are used.

This paper briefly describes the new principle and presents some results attained for resolution, sensitivity, and uniformity using a RSH collimator in clinical practice. Furthermore, typical section images of the facial bones, a hip joint, and a myocardium in vivo are shown. Comparison with SPECT is made on resolution and myocardial imaging.

MATERIALS AND METHODS

Reconstruction Algorithm in Theory

The method described is based on tomosynthesis (27). However to increase the SNR, the projections are processed before summation into a section image. Blur produced by details outside the tomographic section is eliminated by performing a high-pass filtration in a direction tangential to the projection circle (2,26,28). Section thickness is defined through a low-pass filtration in a direction perpendicular to the high-pass filtration (2,26,28).

The number of projections should be at least 60 to achieve an efficient elimination of out-of-section activity (1); in practical situations 64 projections are often registered. This means that the acquisition time is longer than for other RSHT systems, but the total time is not longer than the acquisition time required for SPECT.

Imaging Conditions

Studies were performed on two gamma cameras (Maxicamera 400T and Radicamera, GE Medical Systems, Milwaukee, WI), one with a 39-cm field of view (FOV); the other with a 25-cm FOV, connected on-line to a computer system. The slant-hole collimators (Edc/Septa, Engineering Dynamics Corp., Lowell, MA and GE Medical Systems, Milwaukee, WI) were low-energy general-purpose (LEGP) and unilateral with a slant angle of 30°. The object volume projected by a unilateral rotating collimator results in a reconstruction volume of conical form. The volume obtained with the 30° collimator and the 39-cm FOV gamma camera is sufficient for many clinical applications, whereas the 25-cm FOV camera often yields too small a volume. The slant-hole collimators were rotated manually to register 64 projections. The positioning of the collimators was achieved with an estimated maximum error of $\pm 0.5^\circ$ and $\pm 1.5^\circ$ for the 39-cm FOV and 25-cm FOV camera, respectively.

Due to limitations imposed by the computer software available, it was not possible to use a 128×128 matrix; instead, magnification factors (1.0, 1.6, and 2.0) were used with a 64×64 matrix.

Comparative SPECT studies for resolution and myocardial imaging were performed on the 39-cm FOV gamma camera using standard parallel-hole LEGP collimator and a low-energy high-sensitivity (LEHS) collimator (GE Medical Systems, Milwaukee, WI), respectively.

Reconstruction Algorithm in Practice

Reconstructions were performed with the algorithm outlined above (commercial software will soon be available, Nuclear Diagnostics Co. Ltd., Stockholm, Sweden). The Shepp-Logan filter (29) was used as the high-pass filter function in

all but the myocardial studies, where a Hanning-weighted ramp was used. To obtain uniform voxels, section thickness was chosen to be 1 pixel.

Attenuation correction was made by assuming each section to be parallel to the surface of the object, and lying entirely inside the object. A constant linear attenuation coefficient was used and correction was performed after reconstruction by multiplying each section image by a constant.

SPECT reconstructions were performed with commercially available software (SPETS V06-TSX, Nuclear Diagnostics Co. Ltd., Stockholm, Sweden). The Shepp-Logan filter was used for resolution measurements and a modified form thereof (30) for myocardial data. Attenuation correction was applied.

Measurements

Depth Calibration and Geometric Distortion. A line source phantom was used to calibrate each section image with its distance from the collimator. A plastic tube filled with an aqueous solution of technetium-99m (^{99m}Tc) was placed in grooves milled in a perspex plate. The angle between the two grooves was 45°. Scaling factors at different depths were determined by imaging two parallel line sources (length = 20 cm).

Resolution. Planar system resolution with the 39-cm FOV gamma camera and slant-hole collimator was determined by imaging a line source in air parallel to the collimator face and at different distances from it. Measurements were made with a pixel size of 0.3 cm. The sum of nine count profiles through the line in the registered image was least-squares fitted to a Gaussian curve. From this curve the full width at half maximum (FWHM) was determined.

For the tomographic method described, section resolution, that is resolution within a section image perpendicular to the axis of rotation, and depth resolution, that is resolution between such images, were measured with both line sources and point sources. A line source filled with an aqueous solution of ^{99m}Tc was positioned both in air and a scattering medium (water). The source was orientated perpendicular to the collimator face both on and off the axis of rotation and parallel to the collimator at different distances. Cobalt-57 point sources were placed at different distances from the collimator in air and water. Pixel sizes were 0.3 or 0.6 cm depending on the distance from the collimator.

Resolution measurements using SPECT were also performed. Section resolution was determined using a line source in air and water positioned both on and off the axis of rotation at different distances. SPECT depth resolution was obtained by imaging a line source perpendicular to the axis of rotation.

Resolution was defined as FWHM of least-squares fitted count profiles to Gaussian curves.

Sensitivity. The point sources of known activity used in the resolution measurements were also used to determine system sensitivity.

Uniformity. A cylindrical phantom consisting of a plastic bottle (radius = 4.5 cm, length with constant radius = 16 cm) filled with an aqueous solution of ^{99m}Tc was used to determine uniformity. The phantom was orientated with its long-axis perpendicular to the collimator face. Pixel size was 0.6 cm.

Patients. Three patients referred for routine scintigraphic examination were also imaged. Informed consent was obtained. The facial bones of a female patient were imaged using

the 25-cm FOV gamma camera 3 hr following the administration of 350 MBq ^{99m}Tc -MDP (methylene diphosphonate). The camera was positioned in an anterior view a short distance from the face of the supine patient. Acquisition time was 20 sec per projection; pixel size 0.4 cm. The healthy left hip joint of another female patient was imaged with the 39-cm FOV camera 3 hr after administration of 500 MBq ^{99m}Tc -MDP. The gamma camera was positioned in an anterior view with a 5° cranial tilt ~4 cm from the patient, who lay with her left foot rotated inwards. Acquisition time was 25 sec per projection; pixel size 0.5 cm. A male patient administered 80 MBq thallium-201 during maximum symptom-limited exercise on a bicycle ergometer for cardiac SPECT imaging (31) was also imaged with the method described. The camera was orientated in a left anterior oblique (LAO) 25° position with a 20° cranial tilt in order to achieve an acquisition geometry symmetrical about the long-axis of the left ventricle. Acquisition time was 30 sec; pixel size 0.6 cm. The SPECT images were used for comparison. SPECT acquisition was performed first by rotating the camera through 180°, from left posterior oblique (LPO) 45° to right anterior oblique (RAO) 45°. Acquisition time was 40 sec per projection and 32 projections were registered; pixel size 0.6 cm.

RESULTS

Depth Calibration and Geometric Distortion

The observed depth of each section image from the collimator face was found to satisfy the equation: $y = 1.03x - 0.31$, $r = 1.00$. The observed depth was thus in good agreement with the true. The distance between the two parallel line sources as observed in the section images was 4.2 ($\pm < 0.1$) cm. The scaling factor was found to be constant with depth and geometric distortion negligible.

Resolution

Planar system FWHM increased from 0.8 cm near the collimator face to 2.1 cm at 18 cm.

In Figure 1, section resolution is shown for the tomographic method presented using a line source parallel to the collimator face, in air, and in water. The magnification factor 2.0 (pixel size 0.3 cm) was used for sections closer than ~12 cm from the collimator face. Further away, the magnification factor 1.0 (pixel size 0.6 cm) had to be used, resulting in only half the sampling frequency. Point sources in air situated off the axis of rotation yielded an almost constant section resolution (1.1 ± 0.1 cm at 10 cm from the collimator face). Resolution within each section image is thus assumed to be constant. Section FWHM for the SPECT system using a line source in air decreased from 1.8 cm on the axis of rotation to 1.6 cm peripherally.

For parallel line sources, depth resolution for the new method is shown in Figure 2. Depth resolution was also found to be constant within a section image (2.5 ± 0.2 cm at 10 cm from the collimator face). All point-spread functions were isotropic. Resolution between sections

Section FWHM [cm]

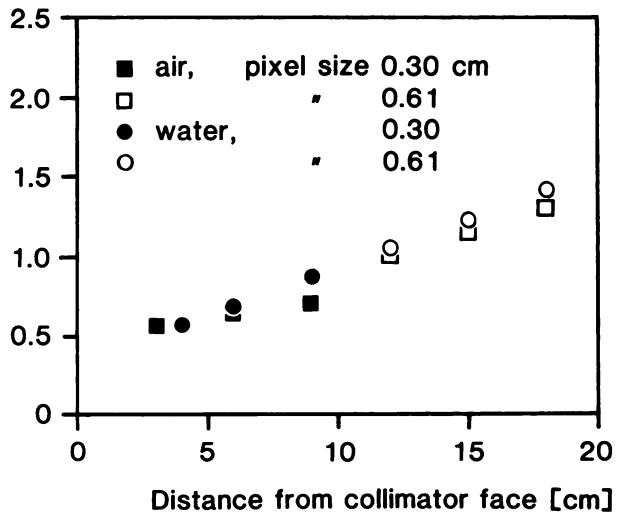


FIGURE 1
Variation in section FWHM in air and water with distance from the collimator face using a line source parallel to the collimator face.

in SPECT was very close to the section resolution (1.9 cm in air and 2.1 cm in water). In Table 1, the results from the resolution measurements are summarized.

Sensitivity

System sensitivity for the 39-cm system was fairly constant with depth: 158 (± 8) cts/MBq, but was slightly lower than for conventional parallel-hole collimators. This is due to the fact that not the whole crystal area is utilized.

Depth FWHM [cm]

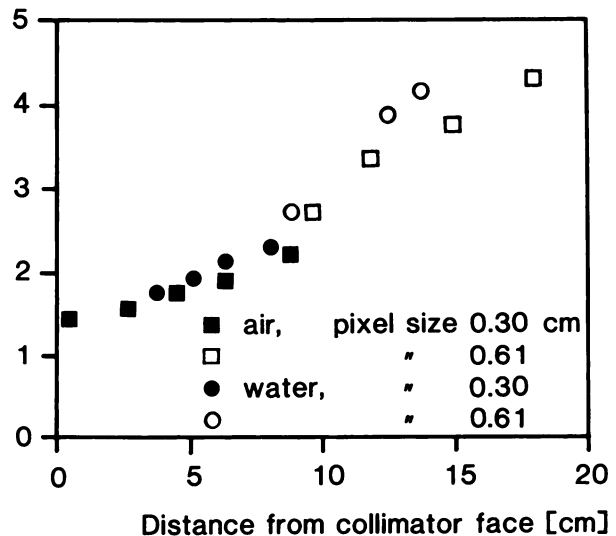


FIGURE 2
Variation in depth FWHM in air and water with distance from the collimator face using a line source parallel to the collimator face.

TABLE 1
Summary of Resolution Measurements Using SPECT and the Method Presented

		Section FWHM			
		Air pixel size		Water pixel size	
		(0.3 cm)	(0.6 cm)	(0.3 cm)	(0.6 cm)
LSF:					
Parallel line source	3 cm	0.6	—	0.6	—
	9 cm	0.7	—	—	0.9
	18 cm	—	1.3	—	1.4
PSF:					
Point sources	3 cm	0.8	—	0.8	—
	9 cm	0.9	—	1.0	—
	18 cm	—	1.8	—	2.0
Perpendicular line source	3 cm	0.9	—	0.9	—
	9 cm	1.1	—	1.2	—
	18 cm	—	1.9	—	2.2
SPECT on AOR [†]		1.8	—	1.9	—
	12 cm off	—	1.6	—	2.1
		Depth FWHM (between sections)			
		Air pixel size		Water pixel size	
		(0.3 cm)	(0.6 cm)	(0.3 cm)	(0.6 cm)
LSF:					
Parallel line source	3 cm	2.2	—	2.2	—
	9 cm	2.6	—	—	3.6
	18 cm	—	5.1	—	5.2
PSF:					
Point sources	3 cm	1.4	—	2.3	—
	9 cm	2.2	—	2.7	—
	18 cm	—	4.3	—	4.5
Perpendicular line source	3 cm	—	—	—	—
	9 cm	—	—	—	—
	18 cm	—	—	—	—
SPECT on AOR		1.9	—	2.1	—
	12 cm off	—	—	—	—

[†] AOR = axis of rotation.

Uniformity

Uniformity, both uniformity within and between sections perpendicular to the axis of rotation, depends on the shape of the object and the position of the section imaged (24–26). In Figure 3, profiles are shown through three reconstructed sections of the cylindrical phantom. The middle section shows an almost correct count profile, while the other two display different degrees of high-pass distortion of an ideal profile.

Patients

Figure 4 shows coronal images of the facial bones; nominal thickness 1.2 cm and separated by 1.2 cm. The four corner spots define the square which circumscribes the circular cross-section through the reconstruction volume. Figure 5 shows coronal section images of a healthy hip joint; nominal thickness 1.0 cm and separated by 1.0 cm. The upper threshold was chosen to reduce the influence of the bladder. It should be noted

that uptake of the isotope in the femoral head and neck was low and that the bone marrow cavity in the femoral bone was clearly visible. Figure 6 shows short-axis images of the heart, i.e., sections perpendicular to the long-axis of the left ventricle; nominal thickness 1.2 cm and separated by 1.2 cm, reconstructed with the method described and SPECT. Note a reduced perfusion in the posterior wall.

DISCUSSION

Depth measurements agree with true distances indicating a regular section image spacing, which is expected for RSH systems.

Planar system resolution alone was slightly inferior to the resolution obtained when the system was used for the tomographic method. Since each projection is high-pass filtered, there is a high-pass distortion of small details whose extension is finite perpendicular to the section (26). This distortion yields a decreased width of

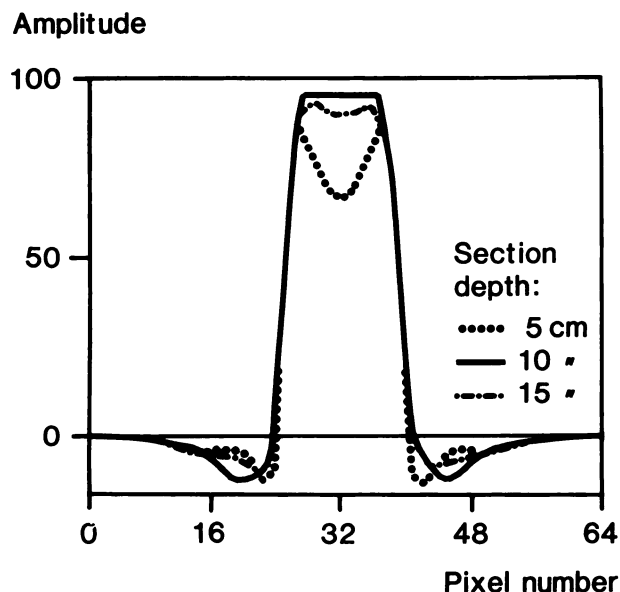


FIGURE 3
Profiles through three reconstructed sections at different depths of a cylindrical phantom. The first section is 5 cm from the collimator face, near one end of the phantom, the second section is 10 cm away, near the middle of the phantom, and the third is 15 cm away, near the other end.

the “point” spread function and hence, a corresponding improvement in resolution for point sources and parallel line sources. The section resolution measured was similar or better to results from other RSHT or SPECT systems.

Depth resolution was slightly better for a point source than for a parallel line source. This is expected since a point source yields a nonsuperimposing distribution for any section image outside the image containing the source. Compared to most other RSHT systems based on iterative reconstruction algorithms, depth resolution of the method is inferior. This indicates that, although more susceptible to noise, an iterative technique is more effective in reducing some of the effects of the empty cone than filtered backprojection. Depth resolution can also be improved if the slant angle of the collimator is increased. For superficial organs such as the thyroid, the bones of the hand, the spine, and the facial bones, it is probably possible to increase the angle to 45° and thereby gain almost a factor of two in depth resolution.

Differences in uniformity between the three profiles of section images of the cylindrical phantom were due to the finite length of the object perpendicular to the section. A reconstructed section will appear high-pass distorted if the projected length of a homogeneous object is less than twice the diameter of the object (26). One way to reduce the distortion could be to use a priori information about the object and modify the filter functions in accordance with this. The high-pass distortion will be perceived as an image enhancement and since our visual system performs high-pass filtration, the qualitative effect of this distortion will not be perceived as very disturbing. Quantitatively, this is of course a disadvantage.

Figure 4 indicates that tomographic facial bone im-

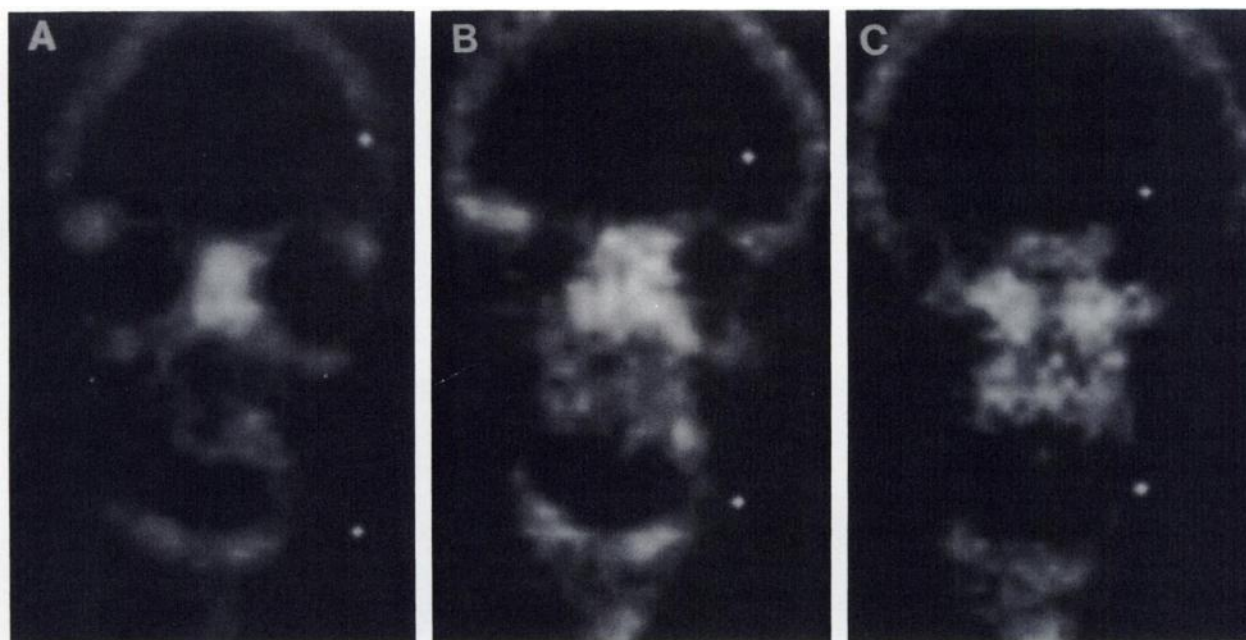


FIGURE 4
Section images of the facial bones; nominal thickness 1.2 cm and separated by 1.2 cm, anterior to posterior. The four corner spots define the square which circumscribes the circular reconstruction area. (A) Anterior section containing part of the frontal bone, the nasal bones, and the jaw bones. (B) Middle section containing the parietal bone, the temporal bone, the cheek bone, and the lower jaw bone. (C) Posterior section consisting mostly of the parietal bone and the temporal bone.

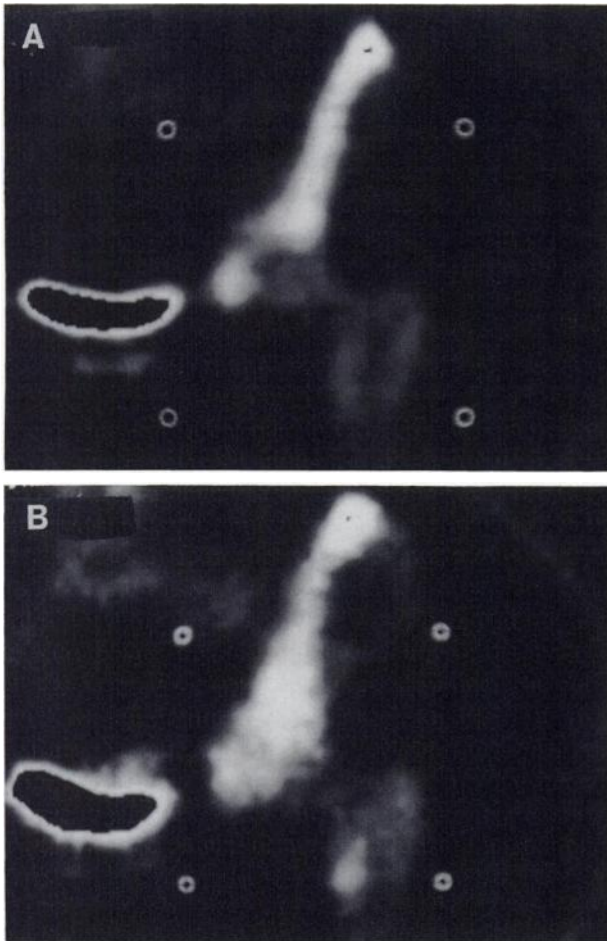


FIGURE 5
Section images of a healthy hip joint; nominal thickness 1.0 cm and separated by 1.0 cm, anterior to posterior. (A–B) The upper threshold was chosen to reduce the influence of the bladder. Note the low uptake of the isotope in the femoral head and neck and the visible bone marrow cavity in the femoral bone.

aging for detection of inflammatory and neoplastic lesion could be performed with the method presented.

Many patients with femoral neck fracture develop complications to healing, which can be diagnosed by detecting a reduced uptake of a bone-seeking radio-

pharmaceutical. Tomographic hip joint imaging with SPECT is difficult because of a concentration of activity in the urinary bladder. Furthermore, the SNR is low in many of the projections due to the large distance between the camera and the hip during acquisition. The images presented indicate that the tomographic method presented should be further investigated for prediction of the healing course in femoral neck fractures.

The myocardium is imaged for detection of ischemic heart disease, localization of coronary artery stenosis, and other diseases affecting the myocardium. The myocardial images show reasonable agreement in information content between the two methods. The difference seen mainly in the inferior wall, is probably explained by the higher attenuation and the effects of scatter in SPECT. A comparative study involving ten patients and extensive phantom measurements which thoroughly evaluates the method for myocardial imaging has been performed (32).

Disadvantages of the method described are due to the empty cone, which causes a relatively poor depth resolution and makes true quantitative determination of the activity distribution impossible. This is a disadvantage which all RSHT systems have in common. Another disadvantage, specific to this method, is that to compensate for the irregular sample density, a weighting function is used which causes image distortion if the projected length of the object is finite with respect to its dimensions parallel to the section.

Advantages include the short and constant distance from the patient to the gamma camera, which is obtained when imaging sections parallel and close to the body surface. This yields a high resolution and SNR compared to SPECT. An advantage specific to the method described is that imaging is not restricted to organs having symmetry about the rotational axis, which allows tomographic imaging of a wider range of organs. Another advantage is the possibility of performing tomographic imaging with a conventional stationary gamma camera and a RSH collimator.

In conclusion, the results obtained from the perform-

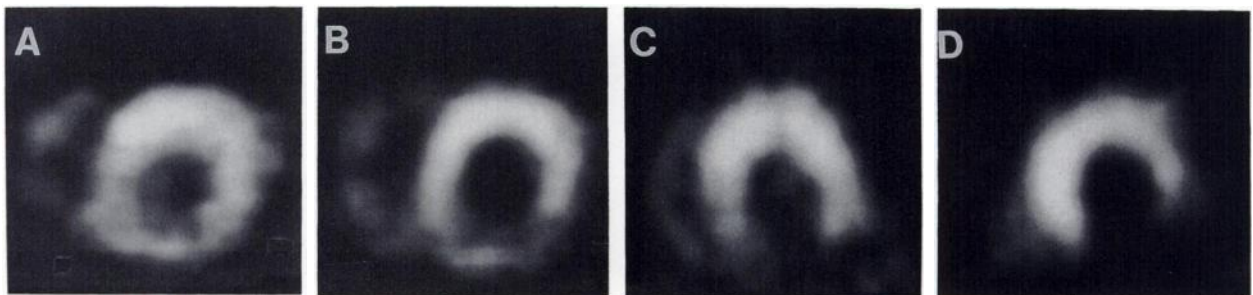


FIGURE 6
Short-axis section images of a myocardium; nominal thickness 1.2 cm and separated by 1.2 cm. Anterior is upwards, posterior downwards, the lateral wall is to the right and the septum to the left. Note the visible right ventricle and reduced perfusion in the posterior wall. (A–B) Tomographic method presented. (C–D) SPECT.

ance evaluation supported by the clinical application images indicate that the new method should undergo further clinical investigation.

ACKNOWLEDGMENTS

The authors thank the heads of and all personnel at the Department of Clinical Physiology at the Thoracic Clinics, Karolinska Hospital, Stockholm and the Department of Hospital Physics, Huddinge Hospital, Huddinge for sharing their equipment and expertise.

This study was supported in parts by grants from the Swedish National Board for Technical Development, Stockholm (project No. 83-04086P).

REFERENCES

1. Edholm P, Granlund G, Knutsson H, Petersson C. Ectomography—a new radiographic method for reproducing a selected slice of varying thickness. *Acta Radiol Diagn* 1980; 21:433–442.
2. Knutsson HE, Edholm P, Granlund GH, Petersson CU. Ectomography—a new radiographic reconstruction method. I. Theory and error estimates. *IEEE Trans Biomed Eng* 1980; 27:640–648.
3. Petersson CU, Edholm P, Granlund GH, Knutsson HE. Ectomography—a new radiographic reconstruction method. II. Computer-simulated experiments. *IEEE Trans Biomed Eng* 1980; 27:649–655.
4. Dale S, Edholm PE, Hellström LG, Larsson S. Ectomography—a tomographic method for gamma camera imaging. *Phys Med Biol* 1985; 30:1237–1249.
5. Freedman GS. Tomography with a gamma camera. *J Nucl Med* 1970; 11:602–604.
6. Muehlehner G. A tomographic scintillation camera. *Phys Med Biol* 1971; 16:87–96.
7. Vogel RA, Kirch D, LeFree M, Steele P. A new method of multiplanar emission tomography using a seven-pinhole collimator and an Anger scintillation camera. *J Nucl Med* 1978; 19:648–654.
8. Gottschalk SC, Smith KA, Wake RH. Tomographic reconstructions with rotating slant hole and seven-pinhole collimators on an Anger gamma camera phantom and clinical studies. In: Paras P, Eikman EA, eds. *Emission computed tomography: the single photon approach*. Rockville, MD: HHS Publication FDA 81-8177; 1981:105–128.
9. Condon B, Mills J, Ardley R, Taylor D. A physical comparison of two fixed-angle emission tomographic cardiac imaging systems. *Phys Med Biol* 1983; 28:131–138.
10. Chang W, Henkin RE. Performance of the rotating slant-hole collimator for the detection of myocardial perfusion abnormalities. *J Nucl Med* 1982; 23:547.
11. Ratib O, Henze E, Hoffman E, Phelps ME, Schelbert HR. Performance of the rotating slant-hole collimator for the detection of myocardial perfusion abnormalities. *J Nucl Med* 1982; 23:34–41.
12. Myers MJ, Busemann Sokole E, de Bakker J. A comparison of rotating slant hole collimator and rotating camera for single photon emission tomography of the heart. *Phys Med Biol* 1983; 28:581–588.
13. Strömquist B, Brismar J, Hansson LI. Emission tomography in femoral neck fracture for evaluation of avascular necrosis. *Acta Orthop Scand* 1983; 54:872–877.
14. Wraight EP, Barber RW, Crossland P, Maltby P. Tomographic images of cerebral blood flow using a slant hole collimator. *Nucl Med Com* 1983; 4:259–263.
15. Coni NK, Wraight EP, Barber RW. Regional cerebral perfusion imaging in the elderly. *Age Ageing* 1984; 13:214–217.
16. Mills JA, Flint J, Taylor DN, Delchar T, McIntosh JA, Pilcher J. Thallium-201 scintigraphy for ischaemic heart disease and infarct detection: comparison of rotating slant-hole tomography and planar imaging. *Br J Radiol* 1985; 58:625–634.
17. Cohen MB, Graham LS, Lake R, et al. Diagnosis of Alzheimer's disease and multiple infarct dementia by tomographic imaging of iodine-123-IMP. *J Nucl Med* 1986; 27:769–774.
18. Nalcioğlu O, Morton ME, Milne N. Computerized longitudinal tomography (CLT) with a bilateral collimator. *IEEE Trans Nucl Sci* 1980; 27:430–434.
19. Rosen PR, Lasher JC, Weiland FL, Kopp DT. Predicting splenic abnormality in Hodgkin's disease using volume response to epinephrine administration. *Radiology* 1982; 143:627–629.
20. Starling MR, Dehmer GJ, Lancaster JL, et al. Segmental coronary artery disease: detection by rotating slant-hole collimator tomography and planar thallium-201 myocardial scintigraphy. *Radiology* 1985; 157:231–237.
21. Lasher JC, Blumhardt R, Kopp DT, Weiland FL. Emission computed tomography: versatile limited angle software. In: Esser PD, ed. *Emission computed tomography: current trends*. New York: Society of Nuclear Medicine; 1983: 211–225.
22. Lancaster JL, Starling MR, Kopp DT, Lasher JC, Blumhardt R. Effect of errors in reangulation on planar and tomographic thallium-201 washout profile curves. *J Nucl Med* 1985; 26:1445–1455.
23. Chang W, Lin SL, Henkin RE. A new collimator for cardiac tomography: the quadrant slant-hole collimator. *J Nucl Med* 1982; 23:830–835.
24. Budinger TF. Physical attributes of single-photon tomography. *J Nucl Med* 1980; 21:579–592.
25. Chiu MY, Barrett HH, Simpson RG, Chou C, Arendt JW, Gindi GR. Three-dimensional radiographic imaging with a restricted view angle. *J Opt Soc Am* 1979; 69:1323–1333.
26. Dale S, Edholm P. Inherent limitations in ectomography. *IEEE Trans Med Imaging* 1988; 7:165–172.
27. Grant DG. Tomosynthesis: a three-dimensional radiographic imaging technique. *IEEE Trans Biomed Eng* 1972; 19:20–28.
28. Dale SM, Edholm PR. Local convolution in ectomography. *IEEE Trans Biomed Eng* 1989; 36:964–968.
29. Shepp LA, Logan BF. The Fourier reconstruction of a head section. *IEEE Trans Nucl Sci* 1974; 21:21–43.
30. Larsson SA. Gamma camera emission tomography. *Acta Radiol Suppl* 1980; 363.
31. Bone D, Holmgren A, Svane B. Thallium tomography in the detection of myocardial perfusion defects. *Acta Med Scand Suppl* 1984; 694:109–119.
32. Dale S, Bone D. Thallium-201 myocardial tomography with a rotating slant hole collimator and a large number of projections. *J Nucl Med* 1990; 31:1682–1688.